

The effect of time-delayed feedback controller on an electrically actuated resonator

S. Shao · K.M. Masri · M.I. Younis

Received: 13 December 2012 / Accepted: 14 May 2013 / Published online: 5 June 2013
© Springer Science+Business Media Dordrecht 2013

Abstract This paper presents a study of the effect of a time-delayed feedback controller on the dynamics of a Microelectromechanical systems (MEMS) capacitor actuated as a resonator by DC and AC voltage loads. A linearization analysis is conducted to determine the stability chart of the linearized system equations as a function of the time delay period and the controller gain. Then the method of multiple-scales is applied to determine the response and stability of the system for small vibration amplitude and voltage loads. It is shown that negative time-delay feedback control gain can lead to unstable responses, even if AC voltage is relatively small compared to the DC voltage. On the other hand, positive time delay can considerably strengthen the system stability even in fractal domains. We also show how the controller can be used to control damping in MEMS, increasing or decreasing, by tuning the gain amplitude and delay period. Agreements among the results of a shooting technique, long-time integration, basin of attraction analysis with the perturbation method are achieved.

Keywords Delayed system · Control · MEMS · Electrostatic force · Multiple scales

1 Introduction

Delay in MEMS devices is a very common phenomenon, which can be introduced into the system unavoidably or by design. In electrostatic MEMS resonators, many inherent system delays can be introduced through actuators, filters, processor dynamics, and feedback measurements. The desire for improved device features, such as low-cost, low-voltage, high quality factor, and improved reliability have motivated great interest to understand the impact of delays on MEMS. On the other hand, feedback controllers have been deliberately used to stabilize the response, compensate for system parameter changes, and generally to enhance the resonator performance [1–5]. Another challenge is to drive electrostatic MEMS resonators at a sharp response while preventing them from collapse due to pull-in.

Several works have been presented recently on time delay feedback controllers. Pyragas [6] presented a delayed feedback controller to stabilize the unstable periodic orbits of a chaotic system. In another work [7], the improved Pyragas controller was shown to stabilize a torsion-free unstable periodic orbit, which conventional methods cannot do. Masoud et al. [8] demonstrated a delayed controller to reduce pendulation on small ship-mounted telescopic cranes. Nayfeh and Nayfeh [9] utilized time-delay acceleration feedback to enhance stability for controlling machine-tool chatter.

S. Shao · K.M. Masri · M.I. Younis (✉)
Binghamton University, State University of New York,
P.O. Box 6000, Binghamton, NY 13902-6000, USA
e-mail: myounis@binghamton.edu

The delayed time in the Pyragas method [6] has been investigated in the case of half of the period of the unstable periodic orbit [10]. Generally, the delayed signal can be displacement, velocity [11], and acceleration [9]. With proper designed time delay, a delayed feedback controller has been proven to stabilize systems including Atomic Force Microscopes (AFM) [12] and magneto-elastic beam systems [13].

Hu et al. [14] studied the dynamics of a controlled Duffing oscillator with delayed feedback with respect to the time delay. Wang and Hu [15] showed that the trivial equilibrium undergoes stability switches as delay time varies. Global stability of displacement feedback [16] and local stability for velocity feedback [17] were studied by using the method of multiple scales and the shooting technique. Also, the analysis on a Single Degree-Of-Freedom (SDOF) system with negative velocity feedback near trivial equilibrium was presented [17], considering quadratic and cubic nonlinearity [18]. It was found that delayed velocity feedback can extend significantly the working frequency ranges of the system compared to with delayed displacement feedback [19]. Delayed feedback of such type was applied to the linear dynamical systems showing that the controller cannot stabilize the unstable motion under some conditions [20].

There are other methods for solving nonlinear dynamic problems with delays, such as energy analysis, which is a combination of the method of Lyapunov's function and the averaging technique, and pseudo-oscillator analysis, which is based on the idea of an oscillator slightly perturbed. Both of them are limited to undamped oscillators, meaning the damping factor is just perturbed into the system [21].

El-Bassiouny [22, 23] presented the analysis of primary and subharmonic resonances of a cantilever beam under time-delay feedback control using averaging and multiple scales methods. A number of important analytical conclusions were reached on the effect of feedback gains, the time-delay, the coefficient of cubic terms, and external excitations [24].

Qaroush and Daqaq [25] utilized a delayed feedback controller to reduce the vibrations of a macro-cantilever beam and a microcantilever sensor. A modified multiple scales perturbation approach demonstrating large time-delay feedback gain was presented. This approach could lead to output peak frequencies not necessarily close to the natural frequency of the system [26]. Erneux [27] investigated strongly nonlin-

ear crane oscillations and lasers subject to optoelectronic feedback by the method of averaging, considering weak damping and weak feedback. Rand et al. [28] utilized a two-variable expansion perturbation scheme to analyze Van der Pol–Hopf bifurcation with delayed feedback. Hamdi and Belhaq [29] investigated non-trivial solutions and bistability in the Duffing oscillator with a delayed displacement feedback via the perturbation method. Nayfeh et al. [30] discussed dynamics of machining using quadratic and cubic stiffness of machine tools, which accounts for the regenerative effects.

In previous works, Younis and Nayfeh [31] used a perturbation method to analytically describe dynamics of a resonant microbeam excited electrically. Alsaleem and Younis [32] investigated theoretically the dynamics of delayed feedback MEMS resonators using a shooting technique and basin-of-attraction analysis and verified their results experimentally [33–35].

In this paper, we use a SDOF model to investigate the dynamics of electrostatic MEMS resonators with the delayed feedback controller of Pyragas [1]. A perturbation method, the method of multiple scales, is used to present analytically the impact on the dynamics of the system by the control gain and delay. The results are then verified using long-time integration, shooting techniques, and basin-of-attraction analysis.

2 Problem formulations

We consider a nonlinear single degree-of-freedom model (Fig. 1) actuated by an electric load composed of a DC component V_{DC} and an AC harmonic component V_{AC} subjected to a viscous damping of coefficient c . The equation of motion governing the behavior of the resonator under a delay feedback controller can be expressed as

$$m \frac{d^2 \hat{x}}{dt^2} + c \frac{d \hat{x}}{dt} + k \hat{x} = \frac{\varepsilon_0 A [V_{DC} + V_{AC} \cos(\hat{\Omega} \hat{t}) + G(\hat{x}_d - \hat{x})]^2}{2(d - \hat{x})^2} \quad (1)$$

In Eq. (1), ε_0 is the dielectric constant of air, A is the electrode area, $\hat{\Omega}$ is the AC excitation frequency, $\hat{x}_d = \hat{x}(\hat{t} - \hat{\tau})$, where $\hat{\tau}$ is the time delay, and G is the amplitude of the velocity feedback controller with unit V s/m (Fig. 2).

Fig. 1 A single degree-of-freedom model of an electrically actuated resonator

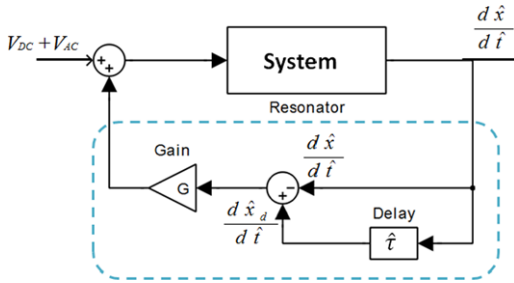
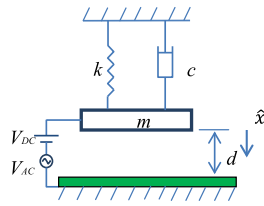


Fig. 2 Schematic for the delayed feedback controller

Next, we normalize Eq. (1) by introducing the nondimensional variables

$$t = \frac{\hat{t}}{T^*}, \quad \tau = \frac{\hat{\tau}}{T^*}, \quad x = \frac{\hat{x}}{d}, \quad x_d = \frac{\hat{x}_d}{d} \quad (2)$$

where $T^* = \sqrt{m/k}$.

Substituting Eq. (2) into Eq. (1) yields

$$\ddot{x} + 2\zeta\dot{x} + x = P \frac{[V_{DC} + V_{AC} \cos \Omega t + G_V(\dot{x}_d - \dot{x})]^2}{(1-x)^2} \quad (3)$$

where $\zeta = \frac{c}{2\sqrt{mk}}$; $\Omega = \hat{\Omega}T^*$; $P = \frac{\epsilon_0 A}{2kd^3}$; $G_V = G \frac{d}{T^*}$.

The nondimensional deflection x can be decomposed as

$$x = \delta + u \quad (4)$$

where δ is the equilibrium position of the oscillator normalized to d , due to V_{DC} and u is the dynamic amplitude of the motion. Substituting Eq. (4) into Eq. (3) yields the governing equation of motion

$$\ddot{u} + 2\zeta\dot{u} + u + \delta = P \frac{[V_{DC} + V_{AC} \cos \Omega t + G_V(\dot{u}_d - \dot{u})]^2}{(1-\delta-u)^2} \quad (5)$$

3 Linearization analysis

Next, we present the linear stability analysis showing vibration characteristics in the neighborhood of the equilibrium position. First, we derive the equilibrium equation of the system in Eq. (5). We set all time-dependent terms equal to zero including the dynamic amplitude u , which leads to

$$\delta = \frac{PV_{DC}^2}{(1-\delta)^2} \quad (6)$$

Equation (6) gives the upper mass position under V_{DC} only. Then we set $V_{AC} = 0$ in Eq. (5). Assuming G_V is small compared to V_{DC} , $\frac{1}{(1-\delta-u)^2}$ in the right-hand side of Eq. (5) can be expanded using a Taylor's series up to the third-order term as

$$\begin{aligned} \frac{1}{(1-\delta-u)^2} &= \frac{1}{(1-\delta)^2} + \frac{2}{(1-\delta)^3}u + \frac{3}{(1-\delta)^4}u^2 \\ &+ \frac{4}{(1-\delta)^5}u^3 + \dots \end{aligned} \quad (7)$$

Also, $[V_{DC} + G_V(\dot{u}_d - \dot{u})]^2$ can be expanded as

$$[V_{DC} + G_V(\dot{u}_d - \dot{u})]^2 = V_{DC}^2 + 2V_{DC}G_V(\dot{u}_d - \dot{u}) + \dots \quad (8)$$

Plugging the linear terms of the right-hand side of Eqs. (7) and (8) into Eq. (5), we obtain

$$\begin{aligned} \ddot{u} + 2\zeta\dot{u} + u + \delta &= \frac{PV_{DC}^2}{(1-\delta)^2} + \frac{2PV_{DC}^2}{(1-\delta)^3}u + \frac{2V_{DC}G_V}{(1-\delta)^2}\dot{u}_d \\ &- \frac{2V_{DC}G_V}{(1-\delta)^2}\dot{u} + \dots \end{aligned} \quad (9)$$

Dropping the equilibrium equation (6) from Eq. (9) and rearranging yield

$$\ddot{u} + 2\zeta_0\dot{u} - 2g\dot{u}_d + \omega^2u = 0 \quad (10)$$

where

$$\zeta_0 = \zeta + g; \quad g = \frac{PV_{DC}G_V}{(1-\delta)^2}; \quad \omega^2 = 1 - \frac{2PV_{DC}^2}{(1-\delta)^3} \quad (11)$$

One can see that ω is the nondimensional natural frequency of the parallel-plate resonator after applying

V_{DC} . The parameter g can be viewed as the nondimensional controller gain.

We should mention that ζ_0 in Eq. (10) cannot be considered as an effective damping ratio. Instead, the term $2\zeta_0\dot{u} - 2g\dot{u}_d$ in Eq. (10) is the complete damping term, because the time delay here is taken into consideration. We need further analysis to uncover the effective damping ratio, which will be presented in Sect. 4.

To study the stability of Eq. (10) we assume the candidate solution to be of the form [36]

$$u = u_0 e^{\lambda t} \tag{12}$$

where u_0 is the amplitude of the solution and λ is the eigenvalue. Note that the delay term is $u_d = u_0 e^{\lambda(t-\tau)}$. Plugging Eq. (12) into Eq. (10) yields the following characteristic equation:

$$\lambda^2 + (2\zeta_0 - 2g e^{-\lambda\tau})\lambda + \omega^2 = 0 \tag{13}$$

Given λ is complex of the form $\lambda = \chi + i\rho$, where χ is the growth or decay rate and ρ is the frequency of oscillations, we split the characteristic equation into real and imaginary parts as

$$\begin{aligned} \chi^2 - \rho^2 + 2\zeta_0\chi - 2g\chi e^{-\chi\tau} \cos(\rho\tau) \\ - 2g\rho e^{-\chi\tau} \sin(\rho\tau) + \omega^2 = 0 \end{aligned} \tag{14}$$

$$\begin{aligned} 2\chi\rho + 2\zeta_0\rho + 2g\chi e^{-\chi\tau} \sin(\rho\tau) \\ - 2g\rho e^{-\chi\tau} \cos(\rho\tau) = 0 \end{aligned} \tag{15}$$

If the real part of the eigenvalue χ is negative, the solution is bounded (stable response) as time increases. On the other hand, a positive real part of the eigenvalue leads to unbounded solution (unstable response). Thus, a zero real part of the eigenvalue, or pure imaginary eigenvalue, defines the linear stability boundary. To solve for this boundary condition, we set $\chi = 0$ in Eq. (14) and Eq. (15) and obtain

$$-\rho^2 - 2g\rho \sin(\rho\tau) + \omega^2 = 0 \tag{16}$$

$$\zeta + g[1 - \cos(\rho\tau)] = 0 \tag{17}$$

Canceling g , we obtain

$$-\rho^2 - 2 \frac{\zeta \sin(\rho\tau)}{1 - \cos(\rho\tau)} \rho + \omega^2 = 0 \tag{18}$$

We can use Eq. (18) to find the system's free oscillation frequency ρ for a specific time delay τ . After

Table 1 The parameters of a parallel-plate capacitor [32, 33]

Parameter	Values
Stiffness k (N m ⁻¹)	320
Electrode separation d (μm)	38
Natural frequency $\hat{\omega}$ (Hz)	193.5
Linear damping coefficient ζ	0.0027
Pull-in voltage (V)	122
Area A (mm ²)	39.6
Effective mass m (g)	0.21
Damping coefficient c (N s m ⁻¹)	0.0014

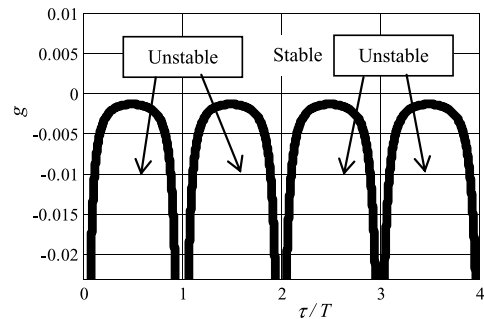


Fig. 3 Stability chart within four periods ($T = 2\pi/\omega$) for $V_{AC} = 1$ V, $V_{DC} = 40.2$ V

obtaining the frequency ρ , we use Eq. (17) to find the effective boundary gain g .

A case study of the capacitive device of [32, 33] of properties of Table 1 is considered. Figure 3 shows the stability chart of this system as a function of the nondimensional effective gain g and time delay τ . In Fig. 3, we obviously can see the periodicity. In one period, for example, the interval between 0 and T , the boundary gain g tends toward negative infinity when τ goes to 0 or T , which can also be seen analytically. When $\tau = 0$ or T , Eq. (16) yields the unique solution $\rho = \omega$, which leads to g having no bounded solution in Eq. (17) because $1 - \cos(\rho\tau)$ is zero.

Also, in Fig. 3, we can see the least possible negative gain to perturb the system into an unstable state is $g = -0.0013$ at $\tau = 0.5T$. In fact, for $\tau = 0.5T$, we have the solutions of Eq. (16) and Eq. (17) as $\rho = \omega, \zeta + 2g = 0$. It indicates that the system needs

$$\zeta + 2g > 0 \tag{19}$$

to reach the stable state.

4 Perturbation analysis

In this section, we use a perturbation method, the method of multiple scales [37], to investigate analytically the response of the resonator for a small motion around the equilibrium position. Therefore, we consider the system is perturbed generating small response $u = O(\varepsilon)$. Considering the terms $V_{DC} = O(1)$, $V_{AC} = O(\varepsilon^3)$, $G_V = O(\varepsilon^2)$ and expanding the electrodynamic term on the right-hand side of Eq. (5) up to the third order, we obtain

$$\begin{aligned} & [V_{DC} + V_{AC} \cos \Omega t + G_V(\dot{u}_d - \dot{u})]^2 \\ &= V_{DC}^2 + 2V_{DC}V_{AC} \cos \Omega t \\ &+ 2V_{DC}G_V(\dot{u}_d - \dot{u}) + O(\varepsilon^4) \end{aligned} \tag{20}$$

Substituting Eqs. (20) and (7) into Eq. (5) yields

$$\begin{aligned} & \ddot{u} + 2\zeta\dot{u} + u + \delta \\ &= P[V_{DC}^2 + \varepsilon^3 2V_{DC}V_{AC} \cos \Omega t \\ &+ \varepsilon^3 2V_{DC}G_V(\dot{u}_d - \dot{u})] \\ &\times \left[\frac{1}{(1-\delta)^2} + \frac{2}{(1-\delta)^3} \varepsilon u + \frac{3}{(1-\delta)^4} \varepsilon^2 u^2 \right. \\ &\left. + \frac{4}{(1-\delta)^5} \varepsilon^3 u^3 \right] \end{aligned} \tag{21}$$

Scaling the damping and dropping the higher order terms beyond the third order in Eq. (21) and the equilibrium terms of Eq. (6) yields the nondimensional equation of motion below

$$\begin{aligned} & \ddot{u} + 2\varepsilon^2 \zeta_0 \dot{u} + \omega^2 u + \alpha_q u^2 + \alpha_c u^3 \\ &= 2\varepsilon^3 f \cos \Omega t + 2\varepsilon^2 g \dot{u}_d \end{aligned} \tag{22}$$

where

$$\begin{aligned} \alpha_q &= -\frac{3PV_{DC}^2}{(1-\delta)^4} \\ \alpha_c &= -\frac{4PV_{DC}^2}{(1-\delta)^5} \\ f &= \frac{PV_{DC}V_{AC}}{(1-\delta)^2} \end{aligned} \tag{23}$$

and the rest of parameters are as defined in Eq. (11).

Since the primary resonance is investigated here, we describe the nearness of the excitation frequency Ω to the natural frequency ω by introducing detuning

parameter σ defined by

$$\Omega = \omega + \varepsilon^2 \sigma \tag{24}$$

Substituting Eq. (24) into Eq. (22), we obtain

$$\begin{aligned} & \ddot{u} + 2\varepsilon^2 \zeta_0 \dot{u} + \omega^2 u + \alpha_q u^2 + \alpha_c u^3 \\ &= \varepsilon^3 2f \cos[(\omega + \varepsilon^2 \sigma)t] + \varepsilon^2 2g \dot{u}_d \end{aligned} \tag{25}$$

The equation above is based on considering the system with small damping, weak quadratic and cubic nonlinearities, weak feedback and soft excitation.

Assuming u is a function of ε and time t , we expand u as

$$\begin{aligned} u(t; \varepsilon) &= \varepsilon u_1(T_0, T_1, T_2) + \varepsilon^2 u_2(T_0, T_1, T_2) \\ &+ \varepsilon^3 u_3(T_0, T_1, T_2) + \dots \end{aligned} \tag{26}$$

where $T_0 = t$, $T_1 = \varepsilon t$, $T_2 = \varepsilon^2 t$.

As will be proven latter, u is independent of T_1 . Therefore the delay term can be written as [36]

$$\begin{aligned} u_d &= u(t - \tau; \varepsilon) \\ &= \varepsilon u_1(T_0 - \tau, T_2 - \varepsilon^2 \tau) + \varepsilon^2 u_2(T_0 - \tau, T_2 - \varepsilon^2 \tau) \\ &+ \varepsilon^3 u_3(T_0 - \tau, T_2 - \varepsilon^2 \tau) + \dots \end{aligned} \tag{27}$$

which upon expansion for small $\varepsilon^2 \tau$ near T_2 becomes

$$\begin{aligned} u(t - \tau; \varepsilon) &= \varepsilon u_1(T_0 - \tau, T_2) + \varepsilon^2 u_2(T_0 - \tau, T_2) \\ &+ \varepsilon^3 u_3(T_0 - \tau, T_2) \\ &- \varepsilon^3 \tau D_2 u_1(T_0 - \tau, T_2) + \dots \end{aligned} \tag{28}$$

Next, we use the following differentiation notations:

$$\frac{d}{dt} \doteq D_0 + \varepsilon D_1 + \varepsilon^2 D_2 + \dots \tag{29}$$

$$\frac{d^2}{dt^2} \doteq D_0^2 + 2\varepsilon D_0 D_1 + \varepsilon^2 (D_1^2 + 2D_0 D_2) + \dots$$

Plugging Eqs. (26)–(29) into Eq. (25) yields

$$\begin{aligned} & [D_0^2 + 2\varepsilon D_0 D_1 + \varepsilon^2 (D_1^2 + 2D_0 D_2)](\varepsilon u_1 + \varepsilon^2 u_2 \\ &+ \varepsilon^3 u_3) + 2\varepsilon^2 \zeta_0 (D_0 + \varepsilon D_1 + \varepsilon^2 D_2)(\varepsilon u_1 \\ &+ \varepsilon^2 u_2 + \varepsilon^3 u_3) + \omega^2 (\varepsilon u_1 + \varepsilon^2 u_2 + \varepsilon^3 u_3) \\ &+ \alpha_q (\varepsilon u_1 + \varepsilon^2 u_2 + \varepsilon^3 u_3)^2 \\ &+ \alpha_c (\varepsilon u_1 + \varepsilon^2 u_2 + \varepsilon^3 u_3)^3 \end{aligned}$$

$$\begin{aligned}
 &= \varepsilon^2 2f \cos(\omega T_0 + \sigma T_2) + \varepsilon^2 2g(D_0 + \varepsilon D_1 \\
 &\quad + \varepsilon^2 D_2)[\varepsilon u_1(T_0 - \tau, T_2) + \varepsilon^2 u_2(T_0 - \tau, T_2) \\
 &\quad + \varepsilon^3 u_3(T_0 - \tau, T_2) - \varepsilon^3 \tau D_2 u_1(T_0 - \tau, T_2)] \quad (30)
 \end{aligned}$$

Spiriting terms of equal power in ε up to the third order gives

$$O(\varepsilon) : D_0^2 u_1 + \omega^2 u_1 = 0 \quad (31)$$

$$O(\varepsilon^2) : D_0^2 u_2 + \omega^2 u_2 = -2D_0 D_1 u_1 - \alpha_q u_1^2 \quad (32)$$

$$\begin{aligned}
 O(\varepsilon^3) : D_0^2 u_3 + \omega^2 u_3 \\
 &= -2D_0 D_1 u_2 - 2D_0 D_2 u_1 - D_1^2 u_1 \\
 &\quad - 2\zeta_0 D_0 u_1 - 2\alpha_q u_1 u_2 \\
 &\quad - \alpha_c u_1^3 + 2f \cos(\omega T_0 + \sigma T_2) \\
 &\quad + 2g D_0 u_1(T_0 - \tau) \quad (33)
 \end{aligned}$$

The solution of Eq. (31) is written as

$$u_1(T_0, T_1, T_2) = A(T_1, T_2)e^{i\omega T_0} + \bar{A}(T_1, T_2)e^{-i\omega T_0} \quad (34)$$

Note that $|A|$ is the amplitude of u_1 . Substituting Eq. (34) into Eq. (32), we obtain

$$\begin{aligned}
 D_0^2 u_2 + \omega^2 u_2 \\
 &= -2i\omega \frac{\partial A}{\partial T_1} e^{i\omega T_0} - \alpha_q (A^2 e^{2i\omega T_0} + A\bar{A}) + \text{cc} \quad (35)
 \end{aligned}$$

where cc represents the complex conjugate terms.

To eliminate the secular term in Eq. (35), we need

$$-2i\omega \frac{\partial A}{\partial T_1} = 0 \quad (36)$$

which indicates that A is the function of T_2 only, $A = A(T_2)$.

Thus, Eq. (35) becomes

$$D_0^2 u_2 + \omega^2 u_2 = -\alpha_q (A^2 e^{i2\omega T_0} + A\bar{A}) + \text{cc} \quad (37)$$

Solving the differential equation above with respect to u_2 yields

$$u_2(T_0, T_2) = \frac{\alpha_q A^2}{3\omega^2} e^{i2\omega T_0} - \frac{\alpha_q A\bar{A}}{\omega^2} + \text{cc} \quad (38)$$

Plugging Eqs. (34) and (38) into Eq. (33) yields

$$\begin{aligned}
 D_0^2 u_3 + \omega^2 u_3 \\
 &= -2i\omega \frac{\partial A}{\partial T_2} e^{i\omega T_0} - 2\zeta_0 i\omega A e^{i\omega T_0} - 2\alpha_q \\
 &\quad \times \left(\frac{\alpha_q A^3}{3\omega^2} e^{i3\omega T_0} + \frac{\alpha_q A^2 \bar{A}}{3\omega^2} e^{i\omega T_0} \right. \\
 &\quad \left. - \frac{2\alpha_q A^2 \bar{A}}{\omega^2} e^{i\omega T_0} \right) - \alpha_c (A^3 e^{i3\omega T_0} + 3A^2 \bar{A} e^{i\omega T_0}) \\
 &\quad + f e^{i\sigma T_2} e^{i\omega T_0} + 2gi\omega A e^{-i\omega\tau} e^{i\omega T_0} + \text{cc} \quad (39)
 \end{aligned}$$

To eliminate secular terms in Eq. (39), we set

$$\begin{aligned}
 2i\omega \frac{\partial A}{\partial T_2} + 2\zeta_0 i\omega A - \frac{10\alpha_q^2 A^2 \bar{A}}{3\omega^2} \\
 + 3\alpha_c A^2 \bar{A} - f e^{i\sigma T_2} - 2gi\omega A e^{-i\omega\tau} = 0 \quad (40)
 \end{aligned}$$

Writing A in the polar form [37] in terms of amplitude a and phase β , $A \equiv \frac{1}{2}a(T_2)e^{i\beta(T_2)}$, yields

$$\begin{aligned}
 i\omega(a' + ai\beta') + \zeta_0 i\omega a - \left(\frac{5\alpha_q^2}{12\omega^2} - \frac{3}{8}\alpha_c \right) a^3 \\
 - f e^{i(\sigma T_2 - \beta)} - gi\omega a e^{-i\omega\tau} = 0 \quad (41)
 \end{aligned}$$

Separating the imaginary and real terms gives

$$\begin{aligned}
 \omega a' + \zeta_0 \omega a - f \sin(\sigma T_2 - \beta) \\
 - g\omega a \cos(\omega\tau) = 0 \quad (42)
 \end{aligned}$$

$$\begin{aligned}
 \omega a\beta' + \left(\frac{5\alpha_q^2}{12\omega^2} - \frac{3}{8}\alpha_c \right) a^3 + f \cos(\sigma T_2 - \beta) \\
 + g\omega a \sin(\omega\tau) = 0 \quad (43)
 \end{aligned}$$

Next, we introduce a new dependent variable $\varphi = \sigma T_2 - \beta$ in order to transform Eqs. (42) and (43) into an autonomous system of equations as below

$$a' = -\zeta_0 a + \frac{f}{\omega} \sin \varphi + ga \cos(\omega\tau) \quad (44)$$

$$\begin{aligned}
 a\varphi' = a\sigma + \left(\frac{5\alpha_q^2}{12\omega^3} - \frac{3}{8\omega}\alpha_c \right) a^3 \\
 + \frac{f}{\omega} \cos \varphi + ga \sin(\omega\tau) \quad (45)
 \end{aligned}$$

Note that a' , φ' are derivatives with respect to T_2 .

For steady-state response, $a' = 0$, $\varphi' = 0$, which yields the following modulation equations governing the amplitude a and phase φ of the dynamic response:

$$-\zeta_0 a + \frac{f}{\omega} \sin \varphi + g a \cos(\omega\tau) = 0 \tag{46}$$

$$a\sigma + \left(\frac{5\alpha_q^2}{12\omega^3} - \frac{3}{8\omega}\alpha_c \right) a^3 + \frac{f}{\omega} \cos \varphi + g a \sin(\omega\tau) = 0 \tag{47}$$

After eliminating variable φ , the steady-state frequency response equation can be expressed as

$$a^2 \left\{ \left[\sigma + g \sin(\omega\tau) + \left(\frac{5\alpha_q^2}{12\omega^3} - \frac{3\alpha_c}{8\omega} \right) a^2 \right]^2 + [g \cos(\omega\tau) - g - \zeta]^2 \right\} = \left(\frac{f}{\omega} \right)^2 \tag{48}$$

For each σ representing the deviation from natural frequency of the excitation frequency, we can obtain the resonance amplitude a by solving Eq. (48). There is possibility that a has three nontrivial solutions, corresponding to the softening or hardening nonlinear behavior. From Eq. (48), we can also notice that $g \sin(\omega\tau)$ accompanies σ , and plays the role of changing the effective excitation frequency. Similarly, $-g + g \cos(\omega\tau)$ plays the role of changing the damping ratio, since it accompanies ζ . Accordingly, an effective damping ratio ζ_e can be defined as shown below:

$$\zeta_e = \zeta + g - g \cos(\omega\tau) \tag{49}$$

Commonly, $\tau = \frac{T_r}{2} = \frac{\pi}{\omega}$ is considered [10] (T_r is the period of the response signal), which according to Eq. (49) gives $\zeta_e = |2g + \zeta|$.

In addition, the solution for u can be expressed as

$$u = a \cos(\omega t + \beta) - \frac{\alpha_q}{2\omega^2} a^2 \times \left[1 - \frac{1}{3} \cos(2\omega t + 2\beta) \right] + \dots = a \cos(\Omega t - \varphi) - \frac{\alpha_q}{2\omega^2} a^2 \times \left[1 - \frac{1}{3} \cos(2\Omega t - 2\varphi) \right] + \dots \tag{50}$$

Note that a and φ are both constant for steady-state response.

5 Small vibrations and the effective damping ratio

Next, we present stability analysis based on the derived equations from the perturbation analysis of Sect. 4. For convenience, we introduce $F_1(a, \varphi)$ and $F_2(a, \varphi)$ to be the right-hand side of Eqs. (44) and (45), respectively. Therefore, Eqs. (44) and (45) are rewritten as

$$a' = F_1(a, \varphi) \tag{51}$$

$$a\varphi' = F_2(a, \varphi) \tag{52}$$

For periodic solutions, a and phase φ need to be constants, (a_0, φ_0) . To determine the stability of the periodic solution, we evaluate the Jacobian matrix of Eqs. (51) and (52) at (a_0, φ_0) as

$$J(a_0, \varphi_0) = \begin{vmatrix} \frac{\partial F_1}{\partial a} |_{(a_0, \varphi_0)} & \frac{\partial F_1}{\partial \varphi} |_{(a_0, \varphi_0)} \\ \frac{1}{a_0} \frac{\partial F_2}{\partial a} |_{(a_0, \varphi_0)} & \frac{1}{a_0} \frac{\partial F_2}{\partial \varphi} |_{(a_0, \varphi_0)} \end{vmatrix} \tag{53}$$

To obtain the eigenvalues, the determinant is set equal to zero

$$|\lambda I - J(a_0, \varphi_0)| = 0 \tag{54}$$

where λ is the eigenvalue and I is the identity matrix. Solving Eq. (54) yields

$$\lambda^2 + R\lambda + S = 0 \tag{55}$$

where

$$R = 2[g - g \cos(\omega\tau) + \zeta] \tag{56}$$

$$S = [g - g \cos(\omega\tau) + \zeta]^2 + \left[\sigma + g \sin(\omega\tau) + \left(\frac{5\alpha_q^2}{4\omega^3} - \frac{9\alpha_c}{8\omega} \right) a_0^2 \right] \times \left[\sigma + g \sin(\omega\tau) + \left(\frac{5\alpha_q^2}{12\omega^3} - \frac{3\alpha_c}{8\omega} \right) a_0^2 \right] \tag{57}$$

We recall that the coefficient of λ in Eq. (55) is equal to the negative sum of the roots, as $R = -(\lambda_1 + \lambda_2)$; and the constant term is equal to the multiplication of the roots, as $S = \lambda_1 \times \lambda_2$. Therefore, the stability condition requires that the real parts of the roots to be negative. Thus, the stability conditions are

$$R = g - g \cos(\omega\tau) + \zeta > 0 \tag{58}$$

$$\begin{aligned}
 S = & [g - g \cos(\omega\tau) + \zeta]^2 \\
 & + \left[\sigma + g \sin(\omega\tau) + \left(\frac{5\alpha_q^2}{4\omega^3} - \frac{9\alpha_c}{8\omega} \right) a_0^2 \right] \\
 & \times \left[\sigma + g \sin(\omega\tau) + \left(\frac{5\alpha_q^2}{12\omega^3} - \frac{3\alpha_c}{8\omega} \right) a_0^2 \right] > 0
 \end{aligned}
 \tag{59}$$

These conditions should be satisfied in order to yield periodic solutions.

Note that the stability condition of Eq. (58) is the same as requiring positive effective damping for the system (see Eq. (49)).

When substituting the values of Table 1 into Eq. (59) we find that $\alpha_c < 0$, $\alpha_q^2 > 0$ and terms including a_0^2 dominate over $\sigma + g \sin(\omega\tau)$. Thus, S is actually always positive. Hence, one concludes that Eq. (58) determines the system’s stability status alone. For $\tau = \frac{T_c}{2} \approx \frac{\pi}{\omega}$, Eq. (58) becomes

$$\zeta + 2g > 0 \tag{60}$$

or $\zeta_e > 0$. It is worth to note that Eq. (60) is the same as Eq. (19).

Next, we prove that ζ_e represents the effective damping of the system. Toward this, the frequency responses of two different systems with the same ζ_e are shown; one is controlled and the other is uncontrolled (Fig. 4). It turns out that they display the same frequency responses. Note that direct long-time integration (LTI) of Eq. (1) is shown as discrete points in Fig. 4, compared to the analytical solution from the method of multiple scales (MMS). One can see they have good agreement. Furthermore, if we generate the time responses at a certain frequency, they appear the same as well (Fig. 5). One can see in Fig. 5 that the two resonators, one controlled and the other uncontrolled, with the same effective damping ratio under the excitation frequency 183 Hz yield the same time responses.

Practically, one can utilize the controller gain g and time delay τ to control the system damping ratio as needed. For a specified τ , g relates to ζ_e linearly. Figure 6 shows the relation for a system with $\zeta = 0.0103$.

Fig. 4 Frequency response curves for $\tau = T/2$ and $V_{AC} = 3.8$ V. (a) $\zeta = \zeta_e = 0.0103$, $g = 0$; (b) $\zeta = 0.0027$, $\zeta_e = 0.0103$, $g = 0.0038$ (triangles: LTI; solid line: MMS)

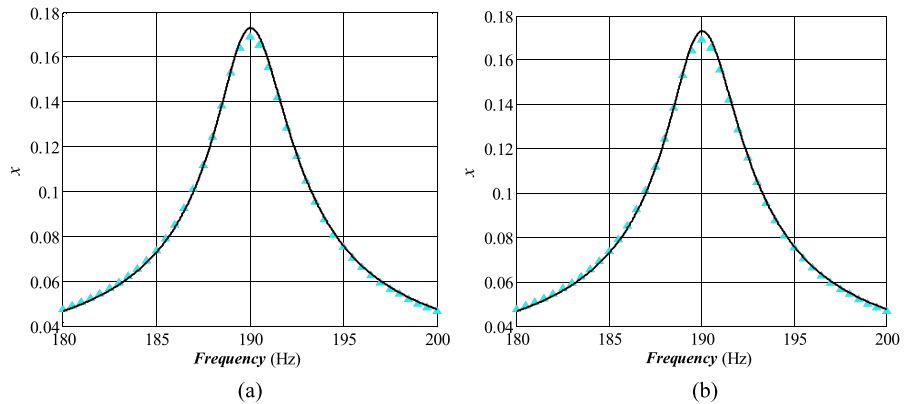
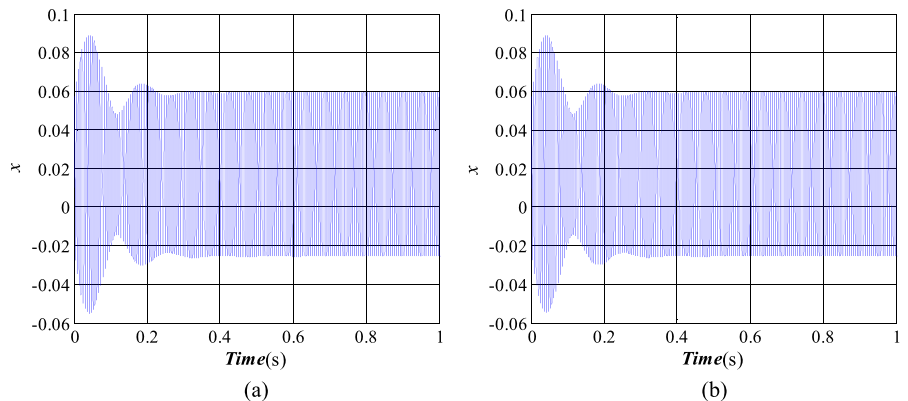


Fig. 5 Time response via LTI at $f = 183$ Hz for (a) $G = 0$, $\zeta = \zeta_e = 0.0103$ and (b) $G = 200$ V s/m, $\zeta = 0.0027$, $\zeta_e = 0.0103$



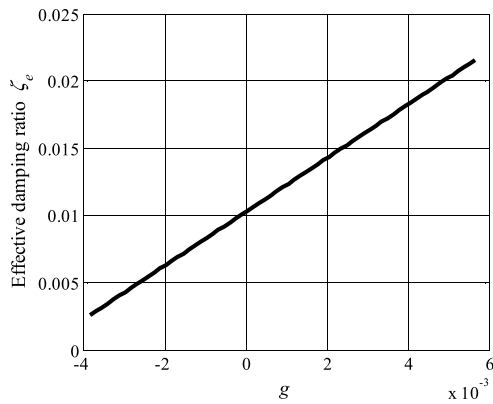


Fig. 6 The effective damping ratio versus the controller gain for $\tau = T/2$

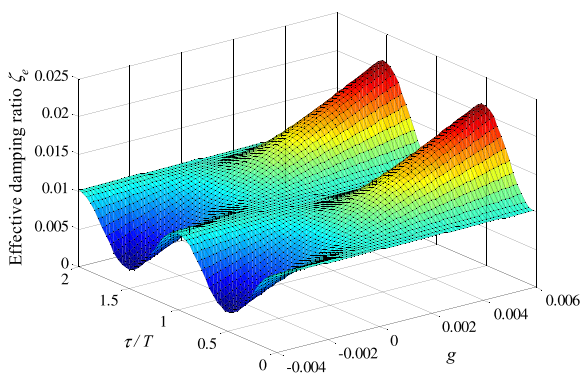


Fig. 7 A 3-D plot for the effective damping ratio versus the controller gain g and the time delay ratio τ/T

In Fig. 7, we show a 3-D plot for the variation of ζ_e as a function of g and τ . One we can see that the variation of ζ_e versus g becomes most significant when the time delay is half the period ($\tau/T = 1/2$) or odd times the period (such as $\tau/T = 1.5$).

6 Moderate and relatively large vibrations

In this section, we investigate the effect of the positive gain on the oscillation response of the capacitive resonator of Table 1. The focus here is on moderate-large response, such that the theories of perturbation and shooting apply. First, we show results for an uncontrolled case with two AC voltage loads. Figure 8 compares the frequency response curve (normalized response versus frequency) obtained by MMS to that of LTI of Eq. (1). For the long-time integration, we use the solution from the previous step as the initial

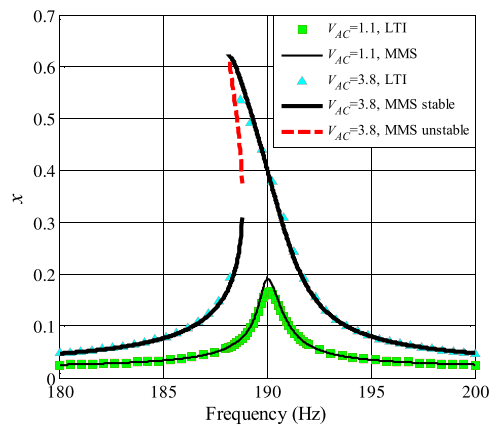


Fig. 8 Frequency-response curves obtained using LTI and MMS for $G = 0$ and $V_{DC} = 40.2$ V for various values of V_{AC} in V

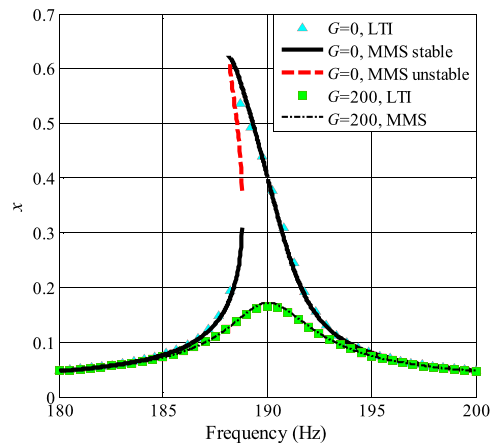


Fig. 9 Frequency-response curves obtained using LTI and MMS for $V_{AC} = 3.8$ V, $V_{DC} = 40.2$ V, and $\tau = T/2$. The unit of G is V s/m

condition to the next frequency step in the frequency sweeping. As shown, the agreement is good among the results of the two approaches.

Figure 9 demonstrates the effect of applying a control gain via both LTI and MMS. It shows that applying a positive control gain instead of lowering the excitation voltage keeps the bandwidth barely changed, while reducing the response amplitude. Therefore, one can use this feature to enlarge the response bandwidth as shown in Fig. 10. This figure compares the uncontrolled response of the resonator to the controlled response using higher values of V_{AC} such that both actuation methods yield the same maximum response amplitude. Clearly, the controlled response has much

larger bandwidth. This remarkable result can be of great advantage in MEMS for sensing and energy-harvesting applications, where both sharp response and wide bandwidth are desirable.

Figure 11 shows the positive gain effect on the time response of the resonator in Fig. 11. The output signal has much smaller overshoot and needs less settling time, although rising time increases under the positive gain controller. From perspective of effective damping ratio, positive gain increases the damping ratio, since $\zeta_e = \zeta + 2g$. Thus, ζ_e is the analytical explanation for the velocity time-delay feedback controller's effects on capacitive resonators.

Next, we investigate the influence of applying a negative gain on the velocity time-delayed feedback controller. Figure 12 shows both numerical LTI results and MMS analytical solution of the frequency response curves for various negative gains from 0–50 V/s/m. This range is equivalent to g from 0 to

–0.0001, which lies inside the stability regime according to Fig. 3. One can see good agreement among all the results. Generally, for a specified excitation frequency, increasing the amplitude of the negative gain G causes the displacement x to increase. In addition, the frequency response curve exhibits nonlinear softening behavior, (Fig. 12), if the negative gain is large enough, such as $G = -50$ V/s/m. Therefore, it can be viewed as an alternative way to generate large response signal instead of simply applying larger harmonic load V_{AC} . From the perspective of damping, these dynamic performances can also be explained by recalling that the time-delay feedback controller with negative gain decreases the effective damping ratio $\zeta_e = \zeta + 2g$.

Figure 13 shows the response amplitude at a fixed excitation frequency $f = 189.5$ Hz while changing the value of the negative gain. The figure shows changes of stability occurring approximately within the inter-

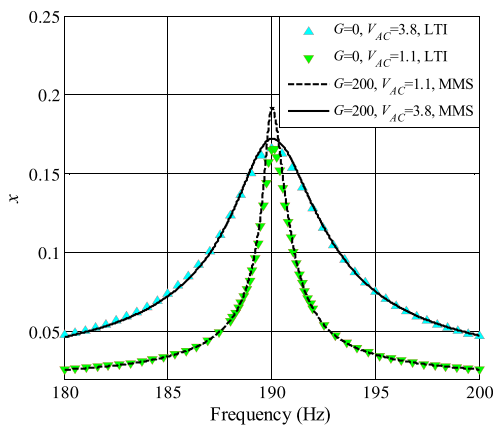


Fig. 10 Frequency-response curves obtained using LTI and MMS for $V_{DC} = 40.2$ V, and $\tau = T/2$. The unit of V_{AC} is V and the unit of G is V s/m

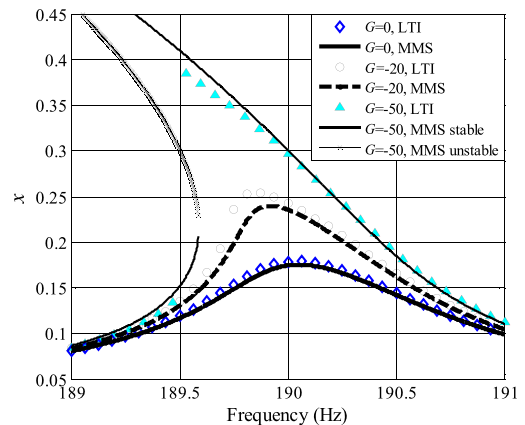
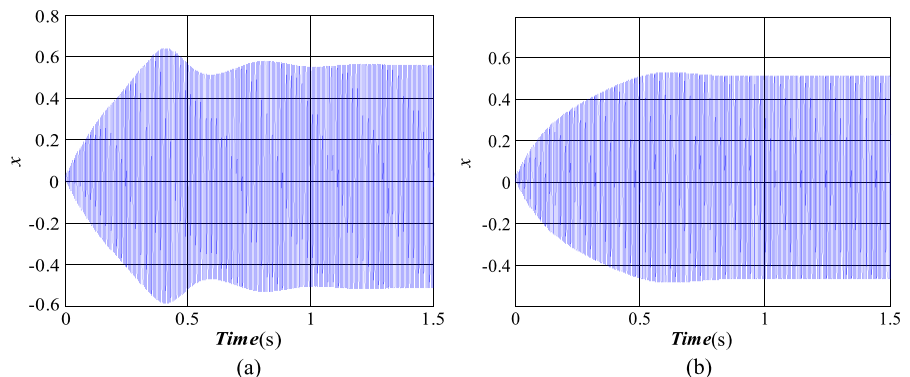


Fig. 12 Frequency response curves obtained using LTI and MMS for various values of negative gain for $V_{AC} = 1$ V, $V_{DC} = 40.2$ V and $\tau = T/2$. The unit is of G is V s/m

Fig. 11 Time responses of (a) uncontrolled system and (b) controlled system, both of which with positive gain $G = 35$ V s/m and $\tau = T/2$ (excitation frequency $f = 188.9$ Hz, $V_{AC} = 5$ V, $V_{DC} = 40.2$ V)



val $G = -40\text{--}70$ V s/m. Some of these instabilities are illustrated in Fig. 14, which shows frequency response curves with different values of relatively large negative gains. Note that when $G < -71$ V s/m, $g < -1.34 \times 10^{-3}$, which means that the system is operated outside the linearized stability boundaries and inside the instability regime of Fig. 3.

The curves of Fig. 14 are obtained using MMS, LTI (when possible), in addition to the shooting technique to find periodic motions combined with the Floquet theory [38]. The shooting technique has the capability of predicting periodic solutions regardless of initial conditions, which is especially advantageous for very weak stability scenarios as in this case. According to the shooting technique, the upper stable branches lose stability through a Hopf bifurcation with one or more Floquet multipliers exiting in the unit circle through complex numbers.

In Fig. 13, if we consider the case of $G = -20$ V s/m, the response curve has a linear shape with

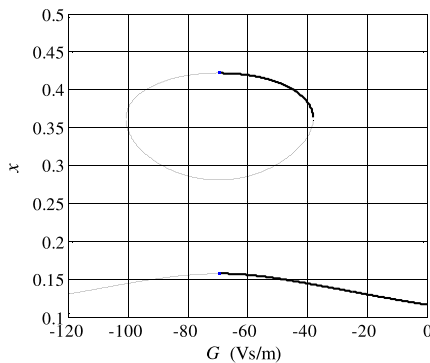


Fig. 13 Gain sweeping response of the MMS solution at $f = 189.5$ Hz, $V_{AC} = 1$ V and $V_{DC} = 40.2$ V (solid line: stable; dashed line: unstable)

no hysteresis. Thus, at $f = 189.5$ Hz, it has one single value of a stable response. When increasing the gain to $G = -50$ V s/m in Fig. 13, the response exhibits softening behavior with hysteresis. Thus, at $f = 189.5$ Hz, the response can be stable of low value, unstable, or stable at higher value. Increasing the gain further to $G = -80$ V s/m (Fig. 14a), according to the perturbation results, the frequency-response curve entirely becomes unstable. The results of longtime integration indicate no stable state between 189–191 Hz, which can be due to not finding the proper initial conditions (due to the very weak basin of attraction in this case). However, it is still able to catch periodic solutions where f is slightly away from natural frequency, shown as diamonds in the plots. The shooting technique, on the other hand, does not suffer from such a problem. Results of the shooting technique in Fig. 14 predict instabilities for specific frequency bands around the primary resonance. One should note that these instabilities refer to the loss of stability of the original periodic (period one) solution. The system loses stability through a Hopf bifurcation, which can be supercritical resulting into two new stable periodic solutions of a frequency that is either commensurate with the excitation frequency or incommensurate with it leading to quasiperiodic motion [39]. These post bifurcation scenarios require further bifurcation analysis, which is outside the scope of this work using, for example, the methods of harmonic balance [39], shooting, or finite difference techniques.

It is worth to mention that this loss of stability of the periodic motion is similar in some sense to the bifurcation reported in [40] in the case of large excitation of electrically actuated microbeams in the softening behavior case. It was reported there that the system loses

Fig. 14 Frequency response curves compared among LTI, MMS and shooting techniques for the resonator with negative controller gains for $V_{AC} = 1$ V, $V_{DC} = 40.2$ V and $\tau = T/2$

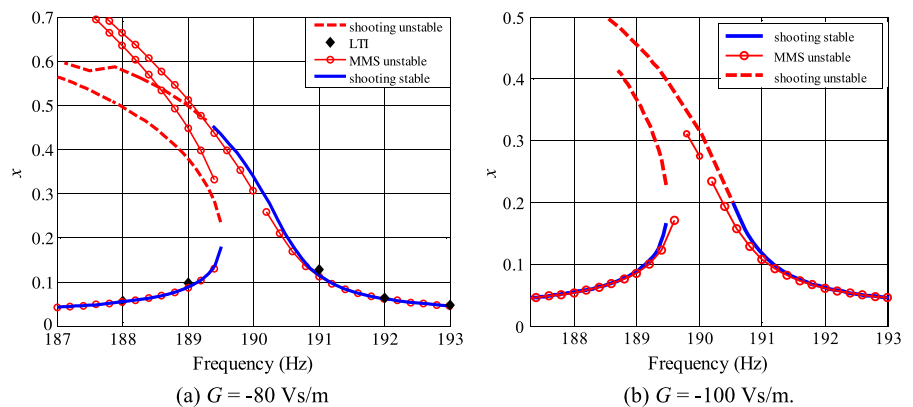


Fig. 15 Time history responses of the uncontrolled system (a) and the controlled system (b) with negative gain $G = -50$ V s/m (excitation frequency $f = 191$ Hz, $V_{AC} = 1$ V)

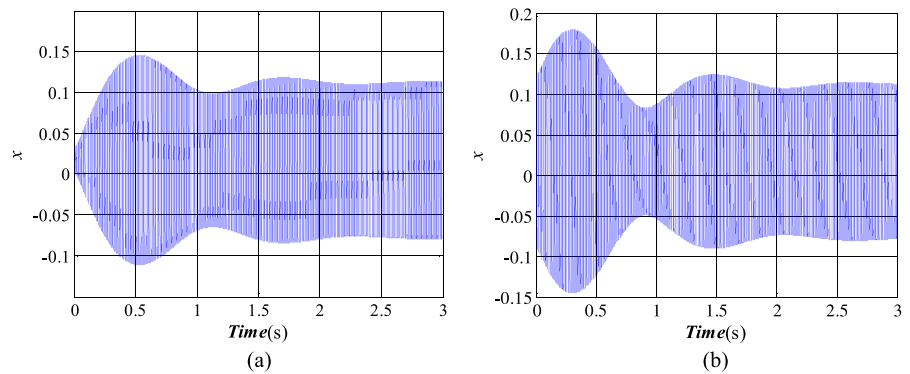
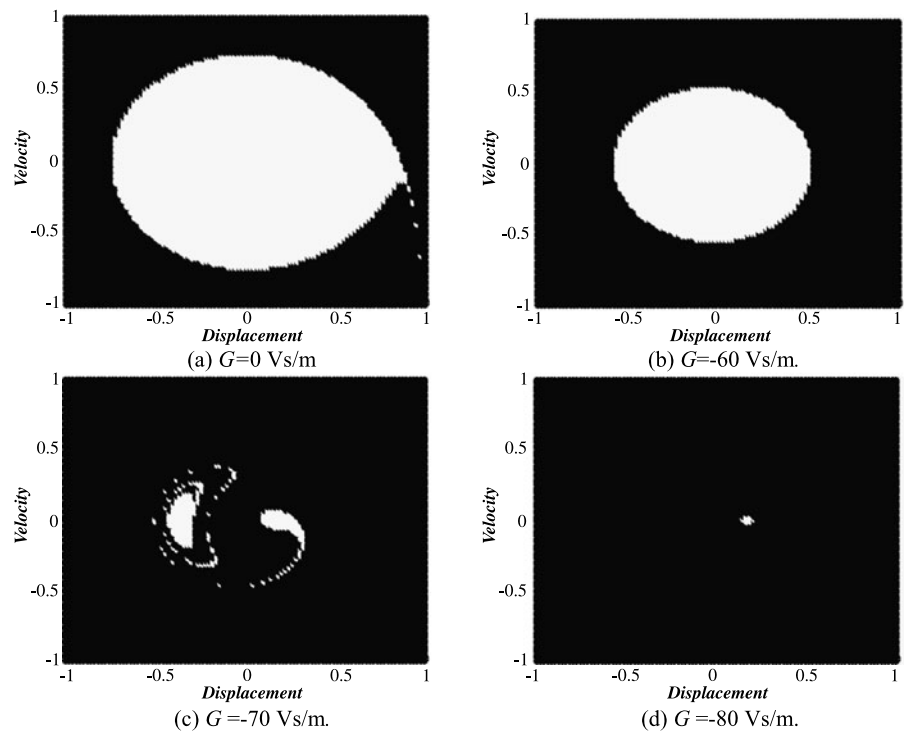


Fig. 16 The basin-of-attraction of the resonator when it is actuated with $V_{DC} = 40.2$ V and $V_{AC} = 1$ V with $\tau = T/2$ at $f = 189.5$ Hz under various values of negative gain



stability through small cascade of period doubling bifurcations, which have very small basins of attractions. The cascade ends with a crisis and vanishes due to the collide with the unstable saddle.

Next, we show examples of the time history response (Fig. 15), which indicates that with a lower effective damping ratio ζ_e , the resonator will have higher overshoot and larger settling time.

The final analysis of this paper is concerned with studying the basin of attraction of the solution [35]. The basin-of-attraction results are obtained by integrating the equation of motion, Eq. (1), in time for various initial conditions using a grid of 500×500 initial

velocity and displacement. The effect of delayed feedback negative gain on resonator stability is shown in Fig. 16. Figure 16a shows the basin-of-attraction before applying the delayed feedback controller, where it is clear that the resonator is stable and has a big safe area. After applying the negative delayed controller gain, the system starts to lose its stability. The safe area decreases when $G = -60$ V s/m and decreases more with $G = -70$ V s/m. Finally, the safe area almost vanishes at $G = -80$ V s/m and the system becomes practically unstable. This fractal behavior is an outcome of the global bifurcation the system experiences as a result of the collide of the stable periodic

orbit with the unstable manifold of the saddle, which results in a multitude of complex dynamical behaviors and the escape from potential well (dynamic pull-in) phenomenon [41, 42].

7 Summary and conclusions

This paper presented analytical solution for a single degree-freedom resonator model actuated by V_{DC} and V_{AC} with a delay feedback controller. The method of multiple scales is used to obtain analytical explanations for the effect of the control gain and delay. We found that positive control gain can enlarge the response bandwidth of the resonator. Another attractive feature in the case of positive gains is achieving the sharp response of resonators while maintaining large bandwidth. This could be very attractive for a variety of sensing and actuation application in MEMS. Negative control gain can bring the resonator nonlinear behavior or make it stronger so that the system may reach an unstable state when the negative gain is large enough, even though the harmonic load V_{AC} is relatively small (for example, $V_{AC} = 1$ V, $V_{DC} = 40.2$ V). This could lead to attractive applications, such as low-actuation voltage MEMS switches.

We compared the results of the perturbation method to the shooting technique and the basin-of-attraction analysis. The shooting technique performs well in predicting the global stability for the resonator under negative gain control. The basin-of-attraction indicated that, while shooting predicts stable regime in the frequency-response curves for large values of negative gain, the basin-of-attraction of these states are extremely small and fragile. Interestingly, the frequency-response curves agreed with the analytical results from MMS, except that MMS predicts unstable solutions everywhere. The various methods used in this paper shed light on the dynamics of delayed-feedback controlled MEMS resonators.

Acknowledgements The authors are thankful to Professor Ali Nayfeh for fruitful discussions on modeling time-delayed systems using perturbation methods. This research has been supported in part by the National Science Foundation (through grant #0846775).

References

- Hu, H., Wang, Z.H.: Dynamics of Controlled Mechanical Systems with Delayed Feedback. Springer, Berlin (2002)
- Balachandran, B., Kalmár-Nagy, T., Gilsinn, D.: Delay Differential Equations: Recent Advances and New Directions. Springer, New York (2009)
- Erneux, T., Kalmár-Nagy, T.: Nonlinear stability of a delayed feedback controlled container crane. *J. Vib. Control* **13**, 603–616 (2007)
- Kalmár-Nagy, T., Stepan, G., Moon, F.C.: Subcritical Hopf bifurcation in the delay equation model for machine tool vibrations. *Nonlinear Dyn.* **26**, 121–142 (2001)
- Kurdi, M.H., Haftka, R.T., Schmitz, T.L., Mann, B.P.: A robust semi-analytical method for calculating the response sensitivity of a time delay system. *J. Vib. Acoust.* **130**, 064504 (2008). doi:[10.1115/1.2981093](https://doi.org/10.1115/1.2981093)
- Pyragas, K.: Continuous control of chaos by self-controlling feedback. *Phys. Lett. A* **170**, 421–428 (1992)
- Pyragas, K., Pyragas, V., Benner, H.: Delayed feedback control of dynamical systems at a subcritical Hopf bifurcation. *Phys. Rev. E* **70**, 056222 (2004). doi:[10.1103/PhysRevE.70.056222](https://doi.org/10.1103/PhysRevE.70.056222)
- Masoud, Z.N., Daqaq, M.F., Nayfeh, N.A.: Pendulation reduction on small ship-mounted telescopic cranes. *J. Vib. Control* **10**(8), 1167–1179 (2004)
- Nayfeh, A.H., Nayfeh, N.A.: Time-delay feedback control of lathe cutting tools. *J. Vib. Control* **18**, 1106–1115 (2012)
- Nakajima, H., Ueda, Y.: Half-period delayed feedback control for dynamical systems with symmetries. *Phys. Rev. E* **58**, 1757–1763 (1998)
- Yamasue, K., Hikiyama, T.: Persistence of chaos in a time-delayed-feedback controlled Duffing system. *Phys. Rev. E* **73**, 036209 (2006). doi:[10.1103/PhysRevE.73.036209](https://doi.org/10.1103/PhysRevE.73.036209)
- Yamasue, K., Hikiyama, T.: Control of microcantilevers in dynamic force microscopy using time delayed feedback. *Rev. Sci. Instrum.* **77**, 053703 (2006). doi:[10.1063/1.2200747](https://doi.org/10.1063/1.2200747)
- Hikiyama, T., Kawagoshi, T.: An experimental study on stabilization of unstable periodic motion in magneto-elastic chaos. *Phys. Lett. A* **211**, 29–36 (1996)
- Hu, H.Y., Dowell, E.H., Virgin, L.N.: Resonances of a harmonically forced Duffing oscillator with time delay state feedback. *Nonlinear Dyn.* **15**, 311–327 (1998)
- Wang, Z.H., Hu, H.Y.: Stability switches of time-delayed dynamic systems with unknown parameters. *J. Sound Vib.* **233**, 215–233 (2000)
- Wang, H.L., Hu, H.Y., Wang, Z.H.: Global dynamics of a Duffing oscillator with delayed displacement feedback. *Int. J. Bifurc. Chaos* **14**, 2753–2775 (2004)
- Wang, H.L., Hu, H.Y.: Bifurcation analysis of a delayed dynamic system via method of multiple scales and shooting technique. *Int. J. Bifurc. Chaos* **15**, 425–450 (2005)
- Wang, H.L., Wang, Z.H., Hu, H.Y.: Hopf bifurcation of an oscillator with quadratic and cubic nonlinearities and with delayed velocity feedback. *Acta Mech. Sin.* **20**, 426–434 (2004)
- Hu, H.Y.: Using delayed state feedback to stabilize periodic motions of an oscillator. *J. Sound Vib.* **275**, 1009–1025 (2004)
- Wang, Z.H., Hu, H.Y.: Stabilization of vibration systems via delayed state difference feedback. *J. Sound Vib.* **296**, 117–129 (2006)

21. Hu, H.Y., Wang, Z.H.: Singular perturbation methods for nonlinear dynamic systems with time delays. *Chaos Solitons Fractals* **40**, 13–27 (2009)
22. El-Bassiouny, A.F.: Fundamental and subharmonic resonances of harmonically oscillation with time delay state feedback. *Shock Vib.* **13**, 65–83 (2006)
23. El-Bassiouny, A.F.: Vibration control of a cantilever beam with time delay state feedback. *Z. Naturforsch. A, J. Phys. Sci.* **61**, 629–640 (2006)
24. El-Bassiouny, A.F., El-Kholy, S.: Resonances of a nonlinear single-degree-of-freedom system with time delay in linear feedback control. *Z. Naturforsch. A, J. Phys. Sci.* **65**, 357–368 (2010)
25. Qaroush, Y., Daqaq, M.F.: Vibration mitigation in multi-degree-of-freedom structural systems using filter-augmented delayed-feedback algorithms. *Smart Mater. Struct.* **19**, 085016 (2010). doi:[10.1088/0964-1726/19/8/085016](https://doi.org/10.1088/0964-1726/19/8/085016)
26. Daqaq, M.F., Alhazza, K.A., Qaroush, Y.: On primary resonances of weakly nonlinear delay systems with cubic nonlinearities. *Nonlinear Dyn.* **64**, 253–277 (2011)
27. Erneux, T.: Strongly nonlinear oscillators subject to delay. *J. Vib. Control* **16**, 1141–1149 (2010)
28. Rand, R.H., Suchorsky, M.K., Sah, S.M.: Using delay to quench undesirable vibrations. *Nonlinear Dyn.* **62**, 407–416 (2010)
29. Hamdi, M., Belhaq, M.: Control of Bistability in a Delayed Duffing Oscillator. *Adv. Acoust. Vib.* **2012**, 872498 (2012)
30. Nayfeh, A.H., Chin, C.M., Pratt, J.: Perturbation methods in nonlinear dynamics—applications to machining dynamics. *J. Manuf. Sci. Eng.* **119**, 485–493 (1997)
31. Younis, M.I., Nayfeh, A.H.: A study of the nonlinear response of a resonant microbeam to an electric actuation. *Nonlinear Dyn.* **31**, 91–117 (2003)
32. Alsaleem, F.M., Younis, M.I.: Integrity analysis of electrically actuated resonators with delayed feedback controller. *J. Dyn. Syst. Meas. Control* **133**, 031011 (2011). doi:[10.1115/1.4003262](https://doi.org/10.1115/1.4003262)
33. Alsaleem, F.M., Younis, M.I.: Stabilization of electrostatic MEMS resonators using a delayed feedback controller. *Smart Mater. Struct.* **19**, 035016 (2010). doi:[10.1088/0964-1726/19/3/035016](https://doi.org/10.1088/0964-1726/19/3/035016)
34. Alsaleem, F.M., Younis, M.I., Ruzziconi, L.: An experimental and theoretical investigation of dynamic pull-in in MEMS resonators actuated electrostatically. *J. Microelectromech. Syst.* **19**, 794–806 (2010)
35. Younis, M.I.: *MEMS Linear and Nonlinear Statics and Dynamics*. Springer, New York (2011)
36. Nayfeh, A.H.: *The Method of Normal Forms*. Wiley, New York (2011)
37. Nayfeh, A.H.: *Introduction to Perturbation Techniques*. Wiley, New York (1981)
38. Nayfeh, A.H., Balachandran, B.: *Applied Nonlinear Dynamics*. Wiley, New York (1995)
39. Daqaq, M.F., Alhazza, K.A., Arafat, H.N.: Non-linear vibrations of cantilever beams with feedback delays. *Int. J. Non-Linear Mech.* **43**, 962–978 (2008)
40. Nayfeh, A.H., Younis, M.I., Abdel-Rahman, E.M.: Dynamic pull-in phenomenon in MEMS resonators. *Nonlinear Dyn.* **48**, 153–163 (2007)
41. Ruzziconi, L., Younis, M.I., Lenci, S.: An electrically actuated imperfect microbeam: dynamical integrity for interpreting and predicting the device response. *Meccanica* (2013). doi:[10.1007/s11012-013-9707-x](https://doi.org/10.1007/s11012-013-9707-x)
42. Ruzziconi, L., Lenci, S., Younis, M.I.: An imperfect microbeam under axial load and electric excitation: nonlinear phenomena and dynamical integrity. *Int. J. Bifurc. Chaos* **23**(2), 1350026 (2013) (17 pages)